Democratic and People's Republic of Algeria

Ministry of Higher Education and Scientific Research

University of Mohamed Boudiaf - M'sila

FACULTY OF TECHNOLOGY
ELECTRONICS DEPARTMENT
N° :……

DOMAIN: SCIENCE & TECHNOLOGY
FILIERE: TELECOMMUNICATIONS
OPTION: SYSTEMS OF TELECOMMUNICATIONS

Dissertation submitted in partial fulfilment of the requirements for the Master degree on Telecommunications Systems

By :

Entitled

Performance Analysis of non-Gaussian Sea Clutter Modelling Using Compound Inverted Exponentiated Rayleigh Distribution

Presented in front of the jury composed by:

Prof. LALAOUI Lahouaoui	**U**niversity of M'sila	Chairperson
Dr. CHALABI Izzeddine	University of M'sila	Supervisor
Dr. SAHED Mohamed	**U**niversity of M'sila	Examiner

Academic year: 2023/2024

Dedication

I want to express my deepest appreciation and gratitude to

Father

Your unwavering support, prayers, and sacrifices have been the foundation, upon which I have built this achievement,

Mom

The woman who has always had my back your love and belief in me has given me the courage to face any challenge thank you for supporting my dreams.

Family and friends and classmates

Those who stood by me, your contribution to my journey is priceless.

Talal and Mounir and Chamsou

Thanks for your advices and support and encouragement

Acknowledgments

Firstly, all praise and thanks are due to Allah, the Most Gracious, and the Most Merciful, for granting me the strength, knowledge, and guidance to reach this momentous occasion.

To my professors and mentor, thank you for your guidance, patience, your advice and help, and for challenging me to think critically, my sincere respect to Dr. Izzeddine CHALABI, as well for the time he spent evaluating and criticizing this work and his total presence during this modest study.

Thanks go to the members of the discussion committee, for kindly accepting the discussion of this master's thesis also for devoting their time to the examination and study of this work.

Our gratitude the Electronics Department teachers of the University of M'sila for turning our obstacles into stepping stones, a special thanks to the Students of the Electronics Department and all those who have contributed far to the end of this work.

Abstract

Radar echo modelling is a major step in the development of robust detection schemes. Compound Gaussian models are largely used to model non-Gaussian radar clutter and provided good results, compound models are characterized by two components speckle and texture, where the speckle component follows Rayleigh law. In this dissertation, the modelling performance of the compound inverted exponentiated Rayleigh (CIER) distribution is tested. A comparative study conducted using the real data of high-resolution sea clutter collected using IPIX radar by McMaster University, Canada. The fitted probability density function (PDFs) and the complimentary cumulative density functions (CCDFs) of the CIER, and the well-known compound K, the compound inverse Gaussian (CIG) distributions are compared with the real PDF and CCDF. The results obtained validate the ability of the CIER distribution to model high-resolution sea clutter.

Key words: Sea clutter, high resolution clutter, modelling.

ملخص

تعتبر نمذجة صدى الرادار خطوة رئيسية في تطوير مخططات كشف قوية. تُستخدم النماذج الغاوسية المركبة على نطاق واسع لنمذجة التشويش غير الغاوسي للرادار وأظهرت نتائج جيدة، حيث تتميز النماذج المركبة بمكونين: الحبيبات والنسيج، ويتبع مكون الحبيبات توزيع رايلي. في هذه الأطروحة، يتم اختبار أداء نمذجة توزيع رايلي الأسى المعكوس المركب (CIER). اجريت دراسة مقارنة باستخدام البيانات الحقيقية لفوضى البحر عالي الدقة الذي تم جمعه باستخدام رادار IPIX من قبل جامعة ماكماستر، كندا. تتم مقارنة دالة الكثافة الاحتمالية المجهزة (PDFs) ودالة الكثافة التراكمية التكميلية (CCDFs) لتوزيع CIER وتوزيع ك المركب المعروف وتوزيع غاوس المركب المعكوس (CIG) مع دالة الكثافة الاحتمالية الحقيقية ودالة الكثافة التراكمية التكميلية. تؤكد النتائج التي تم الحصول عليها قدرة توزيع CIER على نمذجة فوضى بحرية عالية الدقة.

Résume

La modélisation de l'écho radar constitue une étape majeure dans le développement de schémas de détection robustes. Les modèles gaussiens composés sont largement utilisés pour modéliser le fouillis radar non gaussien et ont fourni de bons résultats. Les modèles composés sont caractérisés par deux composantes de speckle et de texture, où la composante de speckle suit la loi de Rayleigh. Dans cette thèse, les performances de modélisation de la distribution composée inverse Rayleigh exponentié (CIER) sont testées. Une étude comparative menée à l'aide de données réelles de fouillis marin à haute résolution collectées à l'aide du radar IPIX par l'Université McMaster, Canada. Les fonctions de densité de probabilité ajustée (PDF) et les fonctions de densité cumulative complémentaires (CCDF) du CIER, K composé et la composée inverse gaussienne (CIG) distributions sont comparés aux réelles PDF et CCDF. Les résultats obtenus valident la capacité de la distribution CIER à modéliser le fouillis marin à haute résolution.

Contents

Abbreviation list

Radar	Radio Detection and Ranging
EM pulse	Electromagnetic pulse
CW	Continuous wave
RCS	Radar Cross Section
UAV	Unmanned aerial vehicle (a kind of drones)
PDF	Probability Density Function
CDF	Cumulative distributed function
CK	Compound K
CP	Compound Pareto
CIG	Compound Inverse Gaussian
CLN	Compound Log-Normal
IR	Inverted Rayleigh
IER	Inverted Exponentiated Rayleigh
CIER	Compound inverted Exponentiated Rayleigh
CCDF	Complimentary cumulative density function
IPIX	Intelligent PIXel Processing
HH	Horisantal polarisation
VV	Vertical polarisation
MSE	Mean square error
KS	Kolmogorov–Smirnov criteria

Figures list

Tables list

General introduction

General introduction

Nowadays, Signal processing has seen a significant increase due to technological development. In remote sensing, Radar designers are tasked with designing innovative and high-performance systems that meet increasingly diverse needs due to these constant and persistent advances. Radar (Radio Detection and Ranging) is an electromagnetic system used to detect and locate objects of interest called targets. The operation of conventional radar involves transmitting an electromagnetic wave and then detecting the echo signal reflected by the target. The primary issue is the degradation of radar detection performance which is inherent to the noise surrounding the target to be detected. This noise, which generally comes from the radar's electronics, is known as the thermal noise and is modeled as Gaussian white noise. Additionally, In order to detect the object, the radar must take in consideration the surrounding environment. Thus, the target signal is immersed in unwanted echoes reflected from the ground and the sea surface. These unwanted signals are referred as clutter. Conventional detectors based on Gaussian hypothesis can provide optimal detection [Weiss1982, Gandhi1994]. In some real situations, the clutter statistics can no longer be modeled by a Gaussian law. This phenomenon occurs, for example, in high-resolution radars and/or operate at low grazing angles. This phenomenon also occurs in areas where the nature of the environment is heterogeneous. This phenomenon is well-described in [Jakeman1976] for sea clutter echoes. In each of these situations, the Gaussian hypothesis is no longer valid. The impulsive behavior of non-Gaussian clutter signals causes a significant increase in false alarms and the detection performance is severely degraded. To address this issue, the radar must adjust its detection threshold to reduce the false alarm rate. In this dissertation, the most focus is particularly will be in sea clutter. Sea clutter is the radar echoes reflected by the sea surface. Modelling these echoes is a crucial step in designing robust radar detectors. Over several years, a number of studies have been conducted on sea clutter modeling. [Trunk1978] addressed this problem. Their demonstration revealed that the statistical measurements of sea clutter have properties that cannot be modelled by a Gaussian law. As a result, they proposed utilizing the Log-normal distribution to describe the statistical variations of sea clutter, which has resulted in remarkable detection performance. In the same context, [Jakeman1976] used Log-normal and K distributions to model sea clutter echoes. The K distribution was further exploited by [Baker1985] and [Watts1985, Watts1987]. Watts' work is related to modeling sea clutter using the K-distribution and then K-plus-noise (considering thermal noise). The Weibull distribution was introduced to describe sea clutter variations in [Lewinski1983]. The successful use of this model extends beyond sea clutter to include other types of clutter, such as ground, sea ice, and atmospheric clutter as presented in [Sekine1990]. Other studies have been conducted in an experimental framework where sea clutter modeling was addressed using real data. In [Farina1997], The Log-normal distribution was found to be effective in modeling real sea

clutter data collected by the IPIX (Intelligent PIXel Processing) radar. For high-resolution radars and/or low grazing angles, the Weibull distribution model offers a good statistical representation of sea clutter [Gini2000, Greco2004]. Several experiments have proved that the K distribution accurately describes high-resolution sea clutter [Farina1997, Gini2000, Greco2004, Ward2006]. Weinberg [Weinberg2013] used the Pareto distribution to describe sea clutter statistics in the presence of thermal noise. In [Farshchian2010, Rosenberg2013], the Pareto-plus-noise distribution was used to model this type of clutter and experimental results were obtained using real data collected by the Australian DSTO (Defense Science and Technology Organization). In [Mezache2015], the Compound Inverse Gaussian (CIG) distribution in the presence of thermal noise is proposed. The IPIX Real data was also used to verify the performance of this model. Recently, in [Chalabi2023], the CIER (compound inverted exponentiated Rayleigh) model is proposed to describe the statistical variation of high-resolution sea clutter. In this manuscript, the modelling performance of the CIER distribution is tested using the IPIX high resolution sea clutter data, the real PDF and CCDF of data are compared with the estimated PDFs and CCDFs of the distributions for different datasets according to the resolution and the antenna polarization.

Chapter I:

Basic radar principles

I.1 Introduction

Radar is an acronym for Radio Detection and Ranging, serves as a vital technology in modern times. It operates on the principle of emitting electromagnetic waves and receives their reflections from objects of interest which called target. This capability enables radar systems to determine the distance, speed, and other characteristics of these targets. For example, the time taken for the waves to travel to the target is used to determine its distance, known as range. Furthermore, radar used the Doppler Effect to assess changes in the frequency of the reflected signal, allowing the calculation of the target's speed. Radar is largely used in many different sectors including aviation, maritime navigation, weather monitoring, and defense. For instance, in aviation, radar assists in air traffic control, ensuring safe navigation and collision avoidance. Similarly, in meteorology, radar is crucial for tracking weather patterns and issuing timely forecasts and warnings. Additionally, radar plays a significant role in military operations, aiding in surveillance, target detection and missile guidance.

I.2 History of radar

The evolution of radar has seen many contributions of numerous researchers across different periods. Among them, Heinrich Hertz's groundbreaking experiments in the late 19th century illuminated the existence of radio waves, laying a foundational understanding for future radar development. Sir Robert Watson-Watt, a Scottish physicist, stands prominently for his demonstration of the first practical radar system in 1935, marking a pivotal moment in radar's evolution. His work was instrumental in shaping radar's role during World War II, alongside the efforts of Sir Henry Tizard and the Chain Home radar team, whose innovations provided crucial early warning capabilities during the Battle of Britain. Albert Einstein's theoretical contributions to electromagnetism further enriched the understanding of radar's underlying principles, while the pioneering research of Charles Townes and Arthur Schawlow on MASER technology in the 1950s paved the way for enhanced radar systems utilizing microwave frequencies. Additionally, the foundational work of Guglielmo Marconi in wireless telegraphy and radio communication during the early 20th century laid essential groundwork for radar's development. Together, these visionary individuals, among others, contributed to radar's transformation from a wartime necessity to a ubiquitous technology with far-reaching applications in both military and civilian domains, as evidenced by its indispensable roles in weather forecasting, air traffic control, and beyond.

I.3 Basic elements of radar

I.3.1 Antenna

The antenna is the most prominent component of the radar system. Its function is to focus the radar's emitted energy in a specific direction. This direction is determined by the elevation and azimuth, which is the angle between the direction of the north and that of the target. Adjustments to the antenna, whether mechanical or electronic, can change this direction, enabling the radar to explore the surrounding area. A bistatic radar system uses two antennas to separate transmission and reception functions. In this setup, the two antennas must always be aligned in the same direction, requiring synchronization or physical connection. Furthermore, minimizing radio-electrical interference is crucial to prevent the strong transmitted signal from disrupting the receiver's operation. These factors contribute to the higher cost of bistatic radar antennas, making monostatic radar generally more preferred.

I.3.2 Duplexer

It is an electronic component that sends a signal to an antenna while the receiver is isolated. On the other hand, the received signal is forwarded to the receiver without being redirected to the transmitter. The complexity of the duplexer depends on the clutter level of the transmitted signal (10 kW to 10 MW) and is related to limiting the leakage of the receiver (the receiver cannot transmit signals above about 100 MW without performance degradation).

I.3.3 Duplexer-Coil-Link

This connection must allow the passage of microwave signals at different locations of the antenna. It includes channels (coaxial and waveguide) and more complex elements that allow the antenna to move. At the antenna level, it can end with various microwave circuits (power dividers, couplers, calculators, phase shifters, etc.).

I.3.4 Transmitter

The active component of the transmitter is the emission tube, which generates the microwave pulse at the specified frequency and power. The transmitter operates as a type of power oscillator. An alternative type of transmitter is the amplifier chain, which boosts the signal through successive stages, starting from about 1W to the final output power, which varies depending on the tube and wavelength used. High-power radar amplifier tubes include klystrons, traveling wave tubes, and crossed-field tubes, while solid-state amplifiers, such as diodes and transistors, are used in the initial power step.

The transmitter also comprises other devices, including cooling systems, power supplies, and control circuits.

I.3.5 Modulator

The modulator is the active component of the transmitter. It stores energy during the intervals between transmissions and releases it during the brief emission period of the radar. The peak power delivered by the modulator is very high, with currents reaching several tens of amperes and voltages of several tens of thousands of volts. The quality of the signals produced by the modulator must be meticulously controlled to prevent any parasitic effects on the emitted signal.

I.3.6 Receiver

It is the most sensitive and complex component of the radar. It is responsible for amplifying and processing the radar signal. Its sensitivity should be very high (up to 10-15 watts). It amplifies the signal without distorting it. The receiver also needs to filter the signal. Its output circuit can be a simple detector.

I.3.7 Synchronizer

The synchronizer ensuring perfect coordination between all components. With a consistently stable clock, it directs operations in real time, distributing signals with high accuracy. It delivers the basic signals which define the transmission times, and various ancillary signals necessary for real-time operations. Its basic element is a very stable clock from which the synchronization signals are generated. These signals are distributed to the different elements.

I.3.8 Indicator

The primary function of the indicator is to provide a visual display of the ranges and bearings of radar targets from which echoes are received. In this basic radar system, the type of display used is the PLAN POSITION INDICATOR (PPI), which is essentially a polar diagram, with the transmitting ship’s position at the center. Images of target echoes are received and displayed at either their relative or true bearings, and at their distances from the PPI center. With a continuous display of the images of the targets, the motion of the target relative to the motion of the transmitting ship is also displayed.

I.4 Radar principles

Radar operation involves navigating through the challenges posed by the environment, particularly in maritime settings where sea clutter becomes a significant factor. Here's an expanded version of the four essential steps.

1. Transmission: The radar emits an electromagnetic pulse (EM pulse) into the surrounding sea surface.

2. Listening Mode: Once the pulse is transmitted, the radar switches to listening mode, anticipating the return signals.

3. Reflection and Sea Clutter: As the transmitted pulse encounters target within its range, it reflects back toward the radar. However, in maritime environments, the radar must deal with sea clutter, which arises from the scattering of radar waves off the surface of the water. This clutter can obscure the detection of the real targets, complicating the radar's task. Advanced signal processing techniques are employed to mitigate sea clutter effects, allowing the radar to separate between clutter and real targets.

4. Echo Reception: Following the encounter with sea clutter and any potential targets, the radar receives echoes of the transmitted pulse. These echoes contain valuable information about the characteristics of detected objects.

In addition to these foundational steps, radar systems employ sophisticated analysis methods to extract relevant parameters from the received echoes. By analyzing properties such as time delay, amplitude and phase, radars can determine crucial information such as the range and velocity of detected targets, despite the presence of sea clutter.

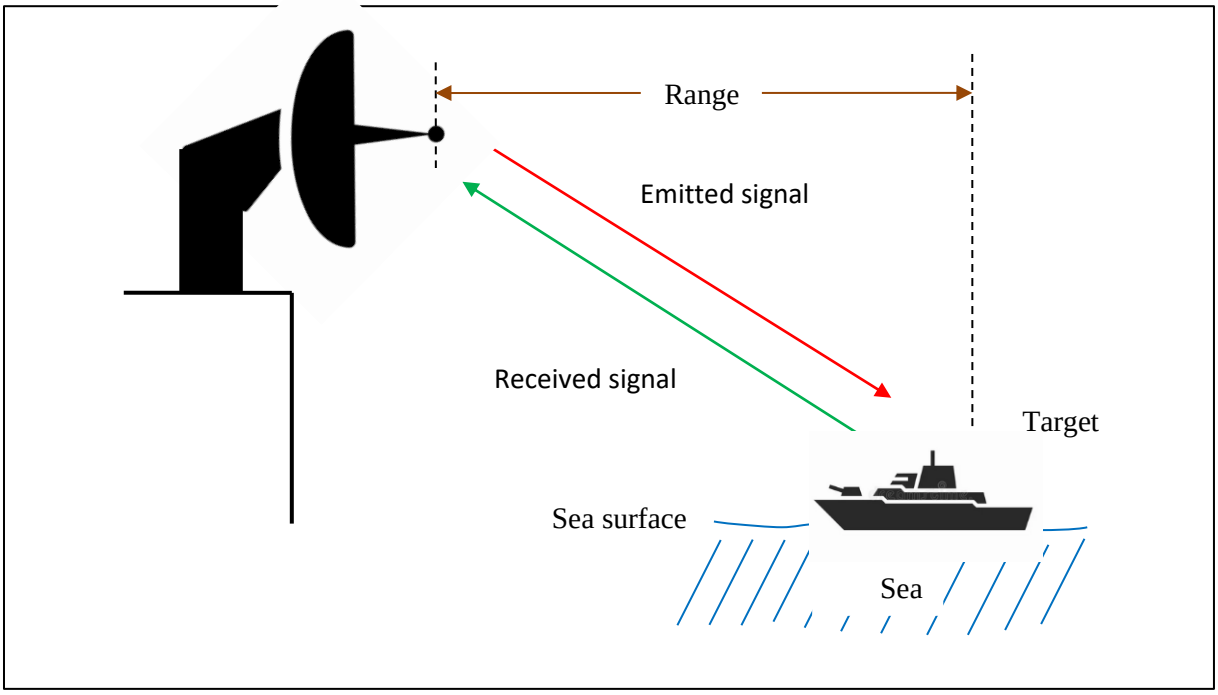

Figure I.1: Basic principle of radar system

I.5 Radar Categorization

I.5.1 Operation

Primary radar is a type of radar system that utilizes radio waves to detect the presence and location of objects such as aircraft, ships, weather formations, and terrain. It operates by emitting radio waves in a particular direction and then detecting the reflected signals from objects in the path of those waves. The time delay between sending the signal and receiving the echo enables the radar system to calculate the distance to the object.

Secondary radar unlike primary radar, which sends out radio waves and listens for echoes, secondary radar involves the radar station sending out interrogation signals to which transponders on aircraft respond.

I.5.2 Illumination

Active radar is a type of radar system that generates its own electromagnetic signals and then detects the reflections or echoes from objects in its vicinity. It operates by emitting continuous or pulsed radio waves towards the target and then receiving the reflected signals. This allows active radar systems to determine the range, bearing, and sometimes the velocity of the target.

Passive radar is a type of radar system that detects and tracked targets by analyzing the reflections of other electromagnetic signals, such as radio or television broadcasts, rather than emitting its own signals. It operates by using multiple receiving antennas to capture signals transmitted by other sources, and then analyzing the differences in these signals to determine the location and movement of objects in the airspace. Passive radar systems offer several advantages, including low probability of interception and detection, as it doesn't emit their own signals, making it suitable for covert surveillance and defense applications.

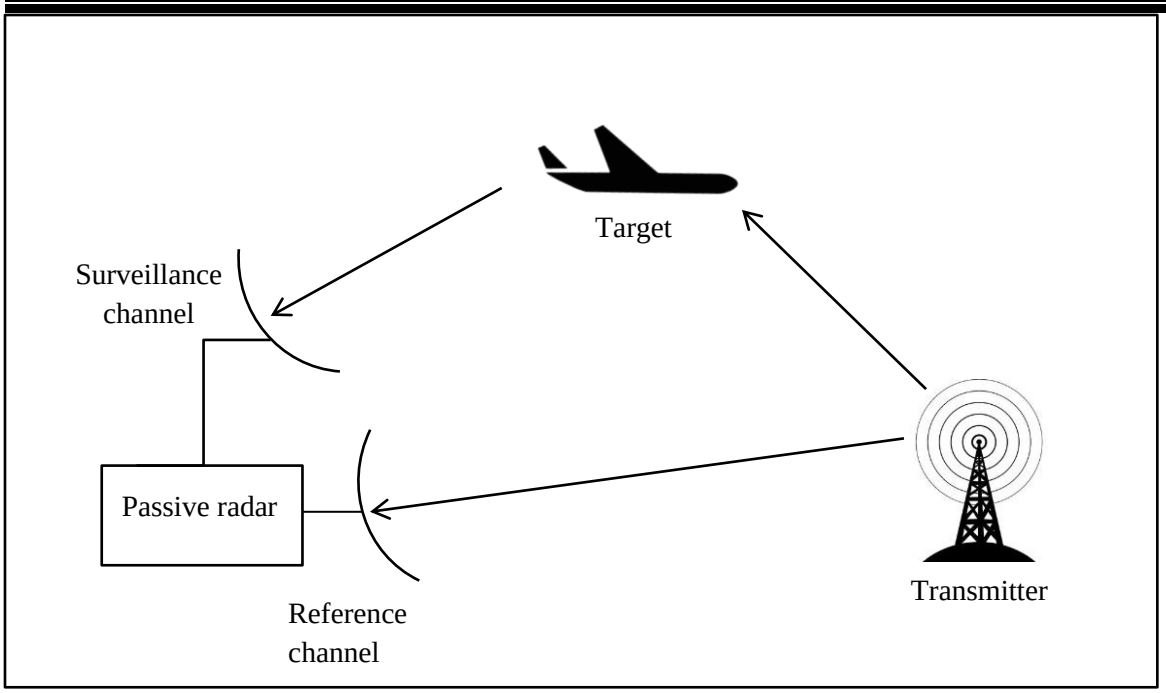

Figure I.2: Active and passive radar systems

I.5.3 Transmission rate

Pulsed radar is a type of radar system that emits short pulses of electromagnetic energy and then listening for the reflected echoes from targets. It allows for precise range measurements and target discrimination.

Continuous wave radar is a type of radar system that emits a continuous waveform without interruption and relies on the Doppler Effect to detect moving targets. It operates by continuously transmitting a radio frequency signal and then comparing the frequency of the transmitted signal with the frequency of the received signal after it has been reflected of the target. Continuous wave radar systems are commonly used in applications such as speed measurement, ground surveillance, and navigation.

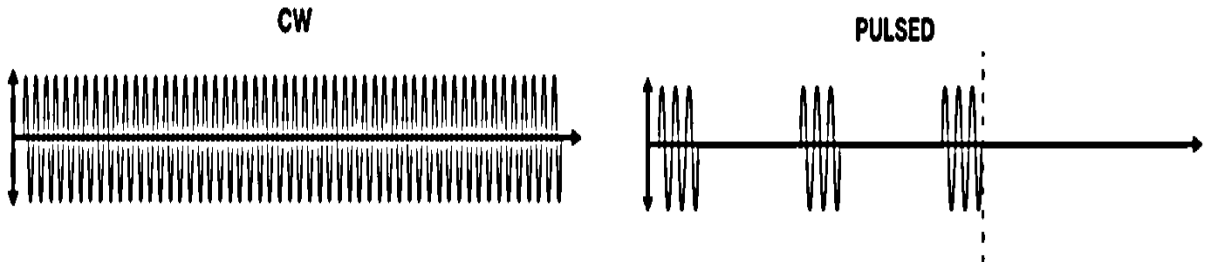

Figure I.3: pulsed and Continuous waves

I.5.4 Geometry:

Monostatic radar is a radar system in which the transmitter and receiver are collocated at the same location. It operates by transmitting a radar signal towards a target and then receiving the reflected signal using the same antenna. Offering advantages such as simplicity of design, lower cost, and the ability to operate in both pulsed and continuous wave modes.

Bistatic radar is a radar system in which the transmitter and receiver are located at different positions. It operates by transmitting a radar signal from one location and receiving the reflected signal at another location using a separate receiver. Bistatic radar systems offer several advantages over monostatic radar, including improved detection performance, reduced vulnerability to electronic countermeasures and increased coverage area. [Richards2014]

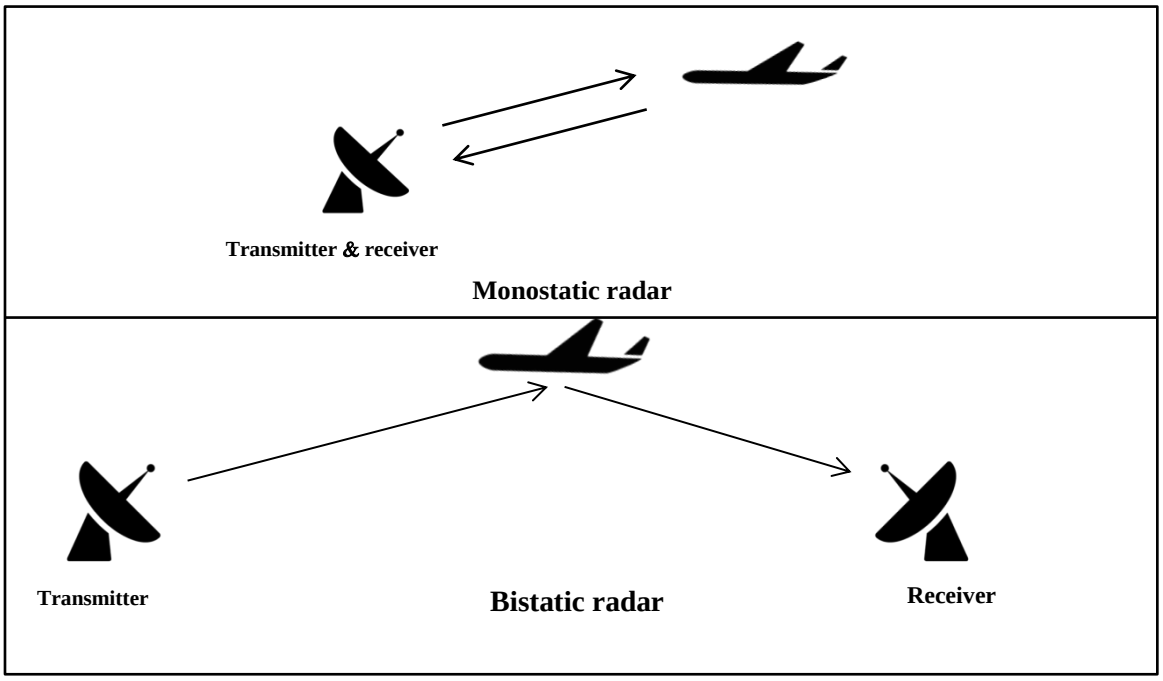

Figure I.4: bistatic and monostatic radar systems

I.6 Radar equation

The radar equation enables the determination of radar's range, based on the technical specifications of the components involved in transmission, the radar apparatus the target and the transmission medium between them, assuming the radar's transmitting antenna is isotropic, meaning it radiates with equal intensity in all directions of space.

Assuming radar equipped with an omnidirectional antenna, emitting energy uniformly in all directions. Given the spherical radiation pattern characteristic of such antennas, the establishment of the peak power density (power per unit area) at any given spatial point, this equation can be derived as follows:

$$P_d = \frac{Peak\ transmitted\ power}{area\ of\ a\ sphere} \quad watts/m^2 \tag{I. 1}$$

In a lossless propagation medium, the density power in a high Range (R) written as:

$$P_d = \frac{p_t}{4\pi R^2} \tag{I. 2}$$

Where p_t is the peak transmitted power and $4\pi R^2$ is the surface area of a sphere of radius R

Characterizing directional antennas will enhance power density in a specific direction as follow:

$$G = \frac{A_e}{\lambda^2} \tag{I. 3}$$

Where G is the gain and A_e is the antenna effective aperture and **λ** is the wavelength

The gain of the arbitrary antenna is the ratio of its maximum power density. The surface power density Pt in the direction of maximum radiation of an antenna expressed according to the following equation:

$$P_d = \frac{P_t\, G}{4\pi R^2} \tag{I. 4}$$

In detection process the radar concentrate energy on the target, the resulting surface currents on the target emit electromagnetic energy in various directions. The emitted energy is directly related to the target's characteristics, including its size, orientation, shape, and material composition, all previous are call them Radar Cross Section (RCS) denoted by σ, and its expression written as:

$$\sigma = \frac{P_r}{P_d} \quad m^2 \tag{I. 5}$$

Where P_r is the power reflected from the target.

The total power supplied to the radar signal processor by the antenna

$$P_{dr} = \frac{P_t G \sigma}{(4\pi R^2)^2} A_e \tag{I. 6}$$

Substituting the value of A_e Equation (I.3) into Equation (I.6**)** giving:

$$P_{dr} = \frac{P_t G^2 \lambda^2 \sigma}{(4\pi)^3 \, R^4} \tag{I.7}$$

Let S_{min} the minimum detectable power from the reception, and R_{max} the radar range [Mahafza2003].

$$R_{max} = \left(\frac{P \, t \, G^2 \lambda^2 \sigma}{(\, 4\pi)^3 S_{min}} \right)^{1/4} \tag{I.8}$$

I.7 Detection theory

I.7.1 Definition

Detection, in the radar context, is the critical process of determining the presence or absence of targets following the reception of the echo signal. This echo signal includes both the desired target and background clutter. The operation involves computing a detection threshold based on the variations in clutter power. Once this detection threshold is established, the received signal is compared to it. If the signal surpasses the detection threshold, it indicates the presence of the target. If the signal fails to exceed the threshold, it suggests the absence of the target.

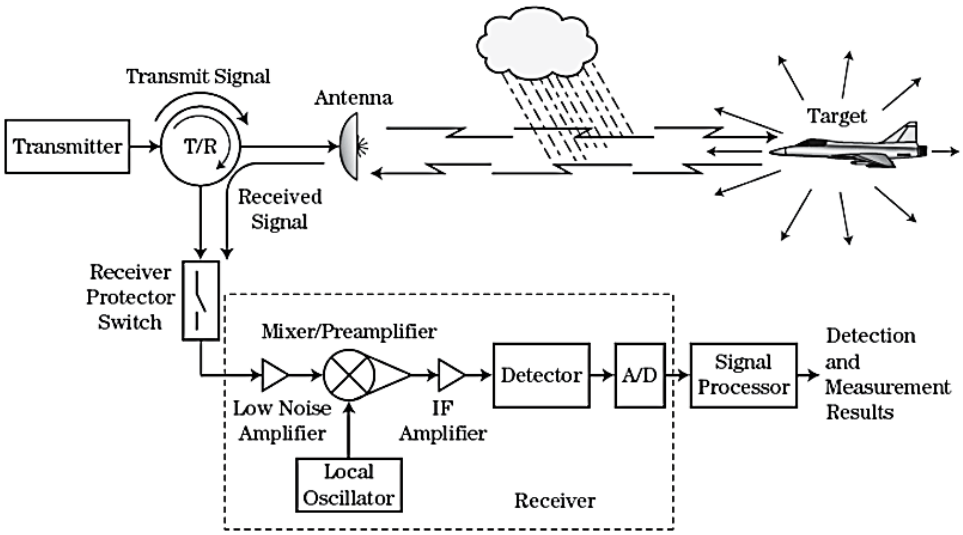

Figure I.5: Detection process

Detection and measurement results in the (Figure I.6) it represent the decision

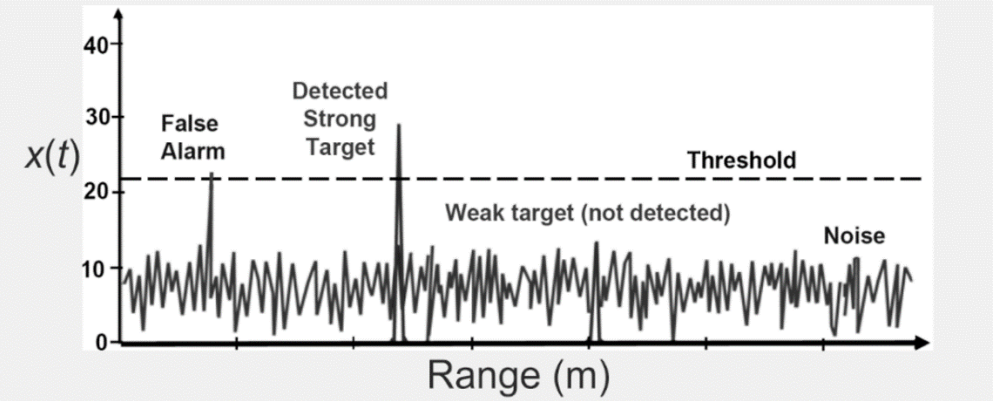

Figure I.6: Example of decision process

There are four possible cases in the decision process because of some detection problems, the randomness of the clutter's nature and the fluctuation of the target are mentioned.

1. ***Target present when the target is actually present:*** This outcome occurs when the radar correctly identifies the presence of the target in the environment. The received signal exceeds the detection threshold, called the detection probability P_D

2. ***Target missing when the target is present:*** This scenario occurs when the radar fails to detect the presence of the target that actually present in the environment , it called the non-detection probability or the probability of Miss $1-P_D$

3. ***Target present when the target is missing:*** This situation arises when the radar incorrectly detects the presence of the target even though no target is actually present. This could occur due to false alarms triggered by noise or clutter in the environment P_{FA}

4. ***Target missing when the target is missing:*** In this case, the radar correctly concludes that no target is present in the environment. The received signal does not exceed the detection threshold, indicating the absence of the target, and this assessment corresponds to the actual absence of the target $1-P_{FA}$. [Echard1991]

I.7.2 Bayes Test

In the context provided, discussing the problem of testing binary hypotheses, where it have to choose between two mutually exclusive hypotheses

I.7.2.1 Prior Probabilities

It started by assuming that it have a prior knowledge about the likelihood of each hypothesis being true before observing any data. These probabilities are known as prior probabilities and are denoted as follows:

- P (H_0) = P_0: The prior probability of hypothesis 0 (Null Hypothesis).
- P (H_1) = P_1: The prior probability of hypothesis 1 (Alternative Hypothesis).

I.7.2.2 Costs associated with decisions

Introduce the concept of costs associated with each possible decision it could make. These costs represent the consequences of each decision depending on the truth of the hypothesis. Formally, if i is a decision, j is the true hypothesis, Cij is the cost associated with decision i given that hypothesis j is true. [Barkat2005]

The Bayes criterion aims to minimize the Bayes risk C by defining decision regions Z_0 and Z_1

$$\mathrm{E[C]} = C_{00}p(D_0, H_0) + C_{10}p(D_1, H_0) + C_{01}p(D_0, H_1) + C_{11}p(D_1, H_1) \qquad (\mathrm{I.9})$$

Every conjoint probability in this expression written in this way:

$$p(D_i, H_j) = p(H_j)p(D_i/H_j) = p(H_j)p(q \in Z_i/H_j) = p(H_j)\int_{Z_i} p_{Q_i/H_j}(q/H_j)dq \qquad (\mathrm{I.10})$$

Observe that the two decision regions are complementary. Hence, it can state:

$$\int_{Z_i} p_{Q_i/H_j}(q/H_j)dq = 1 - \int_{Z_j} p_{Q_i/H_j}(q/H_j)dq \quad , i \neq j, \;\; i,j = 0,1 \qquad (\mathrm{I.11})$$

From the last equation the expression of the average Bayes cost differently as:

$$E[C] = C_{11}p_1 + C_{10}p_0 \int_{Z_0} \left[p_1(C_{01}-C_{11})p_{Q/H_1}(q/H_1) - p_0(C_{10}-C_{00})p_{Q/H_0}(q/H_0)\right] dq \qquad (\mathrm{I.12})$$

Upon observation, it becomes evident that the first two terms in previous equation are not influenced by the decision regions , so minimizing the integral will lead to minimize the average cost $E[C]$ **,** all points in the observation space leading to a negative integral should be allocated to Z_0 while $\Lambda(Q)$ represents the likelihood ratio

$$\Lambda(Q) = \frac{p_{Q/H_1}(q/H_1)}{p_{Q/H_0}(q/H_0)} \underset{H_0}{\overset{H_1}{\gtrless}} \frac{p_0(C_{10}-C_{00})}{p_1(C_{01}-C_{11})} = T \qquad (\mathrm{I.13})$$

I.7.3 Neyman-Pearson test

The Neyman-Pearson test is a statistical method used to make decisions between two hypotheses. Comparing two possible explanations for an observed occurrence and determining which one is more probable based on the available data.

How it works:

- Two Hypotheses: the null hypothesis (denoted H_0) and the alternative hypothesis (denoted H_1). The null hypothesis typically represents the current state or the default assumption, while the alternative hypothesis represents a new or different claim.
- Likelihood Ratio: the Neyman-Pearson test focuses on the likelihood ratio, which is the ratio of the probability of observing the data under the null hypothesis to the probability of observing the data under the alternative hypothesis. Essentially, it's a measure of how much more likely the data are under one hypothesis compared to the other.
- Controlled Error Rates: the test aims to control the probability of making a Type I error (false positive), which occurs when it reject the null hypothesis when it is actually true. This probability is typically denoted by α and is chosen by the experimenter beforehand as the significance level.
- Optimized Decision Rule: the Neyman-Pearson test selects a decision rule that maximizes the probability of making a correct decision P_D while keeping the probability of a Type I error below the specified significance level. This decision rule often involves comparing the likelihood ratio to a critical value or threshold.
- Applications: the Neyman-Pearson test is widely used in various fields such as signal detection theory, medical diagnostics, and quality control, where it's essential to make decisions while controlling error rates effectively.

The decision rule is given as: [Barkat2005]

$$\Lambda(Q) = \frac{p_{Q/H_1}(q/H_1)}{p_{Q/H_0}(q/H_0)} \underset{<}{\overset{>}{}} \lambda \qquad (I.14)$$

λ is the Lagrange multiplier.

I.7.4 Minimax test

The minimax test deals with the difficulty of prior probability knowledge previously experienced. To derive this test, first examine how the choice of threshold affects the Bayes risk. Assuming a fixed decision threshold η, the test's performance relies on comparing the likelihood ratio against this threshold. Consequently, the resulting decision rule from the minimax decision is given as: [Barkat2005]

$$\Lambda(Q) = \frac{(1-p_1)(C_{10}-C_{00})}{p_1(C_{01}-C_{11})} = \eta \qquad \text{(I. 15)}$$

Selecting an appropriate threshold for the P_{FA} and P_M values to ensure equality, the test's result will be certain

$$C_{11}-C_{00} + (C_{01}-C_{11})P_M - (C_{10}-C_{00})P_{FA} = 0 \qquad \text{(I. 16)}$$

I.8 Conclusion

In this chapter, the radar basic principles are presented and explained. The radar technology is based on a complex process that involve mathematical equations, statistical analyses, and advanced algorithms. These processes are essential for detecting targets accurately and making informed decisions. By using mathematical formulas, radar systems calculate the likelihood of detecting targets and the probability of false alarms, which helps in optimizing their performance. Decision-making algorithms analyze the data collected by radar to distinguish between the real detections and false alarms, improving the system's ability to respond effectively in various situations. One of the most important issues in the detection process is the clutter modelling, this issue will be discussed in the next chapter.

Chapter II: Statistical models of high-resolution sea clutter

II.1 Introduction

Sea clutter is a challenge in radar systems operating over maritime environments. Understanding and effectively modeling sea clutter is crucial for radar performance prediction, target detection, and clutter mitigation techniques. With the increasing importance of maritime surveillance, navigation and security, accurate sea clutter modelling becomes pivotal issue for the development of robust radar systems.

The complexity of sea clutter arises from the dynamic and heterogeneous nature of the sea surface, influenced by various environmental factors such as wind speed, wave height, surface currents, and precipitation. Additionally, interference and clutter edge phenomena further contribute to the clutter environment and making its characterization and prediction a complex task [Jakeman1976].

The impulsive character of the signals of a non-Gaussian sea clutter generates a considerable increase in the rate of false alarms and the detection performance is strongly decreased. To remedy this problem, several non-Gaussian distributions are proposed in the radar literature. The next sub-sections will introduce the most performant models used in radar detection.

II.2 Sea clutter modelling

In radar systems, clutter is unwanted echoes that are reflected back to the radar receiver from target of interest environment. These echoes can interfere with radar operations by covering or obscuring the desired signals, making it difficult to detect and track the target accurately. Clutter can be broadly categorized into two main types:

Volume clutter: This type of clutter is created from targets distributed throughout the volume of space being covered by the radar. It includes reflections from rain, atmospheric turbulence, birds, insects, and other airborne particles. Volume clutter can appear as background noise on the radar system, making it challenging to separate between the clutter and the target.

Surface clutter: Surface clutter refers to echoes that arise from targets located on or near the surface of the Earth, such as terrain features, buildings, vegetation and water surfaces.

This research concern the complex phenomenon of sea clutter, which encompasses radar echoes reflected from the sea surface. Accurately modeling of these echoes is crucial for developing sophisticated radar detectors capable of effectively navigating sea clutter environments. Extensive research has revealed that the statistical properties of sea clutter often exhibit non-Gaussian distributions.

The dynamic evolution of the sea can be characterized by two parameters; its state and the direction of the waves. Sea state takes into account the amplitude and distance between waves. Two types of waves appear on the sea surface; capillary waves and gravity waves [Haykin2002]. The first waves are small and numerous, they represent the effect of the wind and they are superimposed on the second which are larger. The speckle is the consequence of the capillarity waves and the texture is the result of the gravity waves. The state of the sea is defined by these two types of waves and the mechanism of reflection of the radar signal on the sea surface is illustrated in Figure II.1 [Haykin2002].

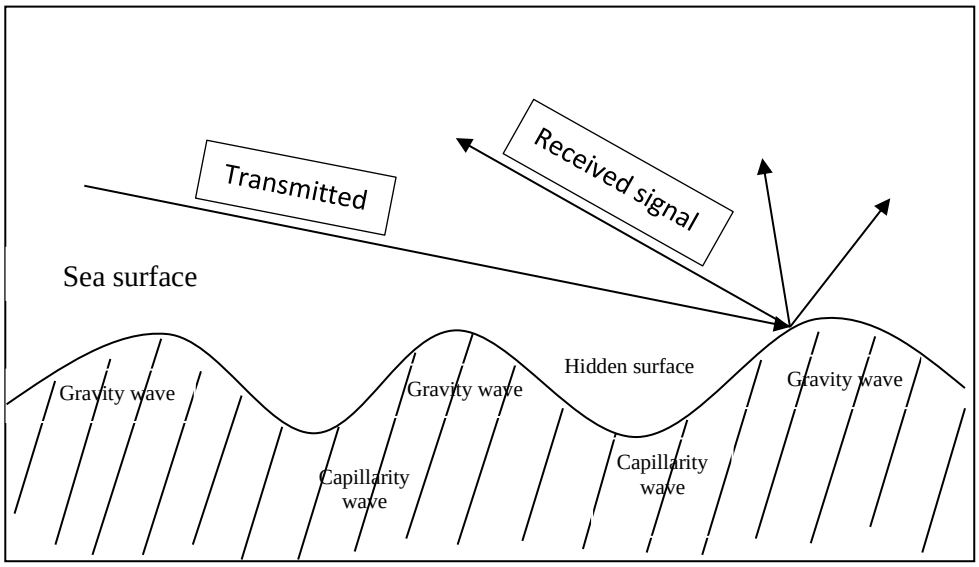

Figure II.1: Radar signal interaction mechanisms (Sea surface)

In the following sub-sections, present the most commonly used models in radar literature for modelling high-resolution sea clutter.

II.2.1 Simple models

II.2.1.1 Log- normal distribution

The Log-normal distribution is characterized by a heavy tail which makes it possible to model non-Gaussian sea clutter, it characterized by its shape parameter σ and scale parameter μ, where μ represents the median clutter amplitude and σ represents the spread or variability of clutter amplitudes [Goldstein1973, Guida1993]. The log-normal PDF given as:

$$p(x) = \frac{1}{x\sqrt{2\pi\sigma^2}}\, exp\left(-\frac{(ln(x)-\mu)^2}{2\sigma^2}\right), \quad x > 0 \qquad \text{(II. 1)}$$

The moments expression of Log-normal distribution is given as:

$$\langle X^n \rangle = exp\left(n\mu + \frac{n^2\sigma^2}{2}\right) \quad \text{(II. 2)}$$

The cumulative distributed function is given as:

$$F(x) = \frac{1}{2}\left(1 + erf\left(\frac{log(x) + m}{\sqrt{2}\sigma}\right)\right) \quad \text{(II. 3)}$$

Where $erf(.)$ is the error function.

II.2.1.2 Weibull distribution

The Weibull distribution was used to model high-resolution sea clutter and it known as a bi-parametric distribution, it characterized by two parameters, the shape parameter b and the scale parameter c [Schleher1976, Fay1977]. The probability density function of the Weibull distribution is given as:

$$p\,(x) = \frac{c}{b}\left(\frac{x}{b}\right)^{c-1} exp\left(-\left(\frac{x}{b}\right)^{c}\right), \quad x \geq 0 \quad \text{(II. 4)}$$

The CDF of this distribution is:

$$F(x) = 1 - exp\left(-\left(\frac{x}{b}\right)^{c}\right) \quad \text{(II. 5)}$$

The expression of the n-order moments of the Weibull distribution is given as:

$$\langle X^n \rangle = b^n \Gamma\left(\frac{n}{c} + 1\right) \quad \text{(II. 6)}$$

Where Γ(.) is the gamma function.

II.2.1.3 Gamma distribution

The texture PDF takes the gamma distribution form as follow:

$$p(x) = \frac{2b^{2\nu}y^{2\nu-1}}{\Gamma(\nu)} exp(-b^2y^2)\,dy \quad \text{(II. 7)}$$

Where ν and b are the shape and the scale parameters.

II.2.2 Compound models

As mentioned previously, the radar sea backscatter is represented by means of two components, which are the speckle component produced by the gravity waves and texture component which is the consequence of the capillary waves [Ward1981, Ward1982], this representation is called compound Gaussian model.

The speckle component follows a Rayleigh law. The overall PDF of compound models is obtained by averaging the speckle component over all possible values of the texture component as follows:

$$p(x) = \int_0^{+\infty} p(x/y)p(y)\,dy \qquad \text{(II. 8)}$$

Where $p(x/y)$ is the PDF of the speckle component and $p(y)$ is the PDF of the texture component.

The speckle component follows a Rayleigh law given as:

$$p\,(x/y) = \frac{\pi x}{2y^2}\ exp\left(-\frac{\pi x^2}{4y^2}\right), \qquad 0 \le x \le +\infty \qquad \text{(II. 9)}$$

II.2.2.1 Compound K distribution

In radar literature, the most common compound model used for modelling high resolution sea clutter is the compound K distribution [Jakeman1976].The texture component of the compound K is gamma distributed as:

$$p\,(y) = \frac{2b^{2v}y^{2v-1}}{\Gamma(v)}\ exp(-b^2y^2), \qquad 0 \le x \le +\infty \qquad \text{(II. 10)}$$

Where ν and b are the shape and the scale parameters. Γ (.) is the gamma function.

Substituting (II.9) and (II.10) in (II.8) and after some mathematical simplifications, the CK PDF is obtained as follow

$$p\,(x) = \frac{4c}{\Gamma(v)}(cx)^v K_{v-1}(2cx) \qquad \text{(II. 11)}$$

Where $c = b\sqrt{\pi/4}$ the scale parameter, $K_{v\text{-}1}(.)$ is the modified Bessel function of the order (v-1)

The statistics of the compound K distribution are fully defined by the shape parameter ν and the scale parameter c. The shape parameter ν describes the state of the sea. The values for this parameter belong to the interval [0.1, ∞ [. If ν tends towards 0.1, the clutter is very spiky, which results in a long tail of the distribution. This is explained by the presence of a high number of intense echoes. If ν tends tend to infinity, the compound K distribution simply becomes a Gaussian distribution. The scale parameter c is a positive constant, responsible for variations in the mean level of the clutter.

The CDF of the CK distribution is expressed in terms of the Bessel function as follows:

$$F(x) = 1 - \frac{2}{\Gamma(v)}(cx)^{v} K_{v}(2cx) \qquad \text{(II. 12)}$$

The moment expression of the CK distribution of order n is given by:

$$\langle X^{n} \rangle = \left(\frac{4}{\pi b^{2}}\right)^{n} \frac{\Gamma(n+1)\Gamma(v+n)}{\Gamma(v)} \qquad \text{(II. 13)}$$

II.2.2.2 Compound Pareto distribution

The compound Pareto (CP) distribution is a statistical model used to describe certain types of data, particularly in the context of sea clutter. It has been used in some studies for its analytical simplicity compared to other distributions like the compound K distribution [Weinberg2013, Rosenberg2013].

In this model, there are two key parameters; the shape parameter α and the scale parameter β. These parameters govern the characteristics of the distribution. The shape parameter determines the shape of the CP distribution component, which typically describes the slowly varying clutter elements. The scale parameter controls the intensity of the clutter PDF. The overall PDF of the CP is obtained in a similar way as the CK distribution, except that in this case the texture follows the inverse Gamma distribution as follow

$$p\,(y) = \frac{\beta^{\alpha}}{\Gamma(\alpha)} y^{-\alpha-1} exp\left(-\frac{\beta}{y}\right) \qquad \text{(II. 14)}$$

Substituting (II.14) and (II.9) in (II.8), the compound Pareto distribution PDF without noise expression shown as follow:

$$p(x) = \frac{\alpha\beta^{\alpha}}{(x+\beta)^{\alpha+1}} \qquad \text{(II. 15)}$$

The corresponding CDF is expressed as follows:

$$F(x) = 1 - \left(\frac{\beta}{x+\beta}\right)^{\alpha} \qquad \text{(II. 16)}$$

The moments expression of order n associated with the compound Pareto distribution are given by:

$$\langle X^n \rangle = \frac{\beta^n \Gamma(r+1)\Gamma(\alpha-n)}{\Gamma(\alpha)} \qquad \text{(II. 17)}$$

II.2.2.3 CIG distribution

The Compound Inverse Gaussian distribution has introduced for modeling high resolution sea clutter [Mezache2015]. Experimental results indicate that this model performs well (in capturing a real data from the IPIX radar system). The CIG distribution comprises two components: speckle and texture. PDF of the CIG distribution is derived similarly to compound K and compound Pareto distributions. In this case, the texture component follows an Inverse Gaussian distribution, as described by [Mezache2015].

$$p(y) = \frac{\lambda^{1/2}}{\sqrt{2\pi}\gamma^{3/2}} exp\left(-\lambda\frac{(y-\mu)^2}{2\mu^2 y}\right), \qquad 0 < y < \infty \qquad \text{(II. 18)}$$

Where λ is the shape parameter and μ is the mean. The values of the shape parameter λ are defined in the interval [0.1, ∞ [, with λ ∈ [0.1, 1] for spiky clutter and as λ tends to infinity the CIG distribution tends towards the Exponential distribution. By substituting equations (II.18) and (II.9) into equation (II.8), the PDF of the CIG distribution is obtained as follows:

$$p(x) = \sqrt{\frac{\lambda\pi}{2}}\frac{x}{2}\int_0^{+\infty} y^{-\frac{7}{2}}\, exp\left(-\frac{\pi x^2}{4y^2} - \lambda\frac{(y-\mu)^2}{2\mu^2 y}\right) dy \qquad \text{(II. 19)}$$

The CDF of the CIG distribution is given by

$$F(x) = 1 - \left(1+\frac{2x}{\lambda}\right)^{-\frac{1}{2}} exp\left(\frac{\lambda}{\mu}\left(1 - \sqrt{1+\frac{2x}{\lambda}}\right)\right) \qquad \text{(II. 20)}$$

The expression of the n-order moments of the CIG distribution is given as follows:

$$\langle X^n \rangle = \Gamma(n+1)\sqrt{\frac{2\lambda}{\pi\mu}}\mu^n e^{\lambda/\mu} K_{n-1/2}\left(\frac{\lambda}{\mu}\right) \quad \text{(II. 21)}$$

II.2.3 Compound models in presence of thermal noise

Thermal noise is the random fluctuation of voltage within electrical components such as a resistor due to the thermal motion of electrons. The power spectral density of thermal noise is practically flat over a very large band of frequencies. This noise is inherent in all electronic devices and communication systems, setting a fundamental limit on their performance.

In presence of additive thermal noise, the speckle component is affected by an increase in its average power and the speckle PDF is given as [Watts1987]:

$$p(x/y) = \frac{x}{\sigma^2+2y^2/\pi}\, exp\left(-\frac{x^2}{2\sigma^2+4y^2/\pi}\right) \quad \text{(II. 22)}$$

Where $2\sigma^2$ is the thermal noise power.

II.2.3.1 Compound K distribution

Substituting (II.20) and (II.10) in (II.8), the overall PDF of the compound K distribution is given as [Watts1987]:

$$p(x) = \int_0^{+\infty} \frac{x}{\sigma^2+2y^2/\pi}\, exp\left(-\frac{x^2}{2\sigma^2+4y^2/\pi}\right)\frac{2b^{2v}y^{2v-1}}{\Gamma(v)}\, exp(-b^2y^2)\, dy \quad \text{(II. 23)}$$

II.2.3.2 CIG distribution

The thermal noise added to the compound inverse Gaussian distribution [Mezache2015], the PDF takes the form:

$$p(x) = \int_0^{+\infty} \frac{x}{\sigma^2+2y^2/\pi}\, exp\left(-\frac{x^2}{2\sigma^2+4y^2/\pi}\right)\frac{\lambda^{\frac{1}{2}}}{\sqrt{2\pi}y^{\frac{3}{2}}} exp\left(-\lambda\frac{(y-\mu)^2}{2\mu^2 y}\right) dy \quad \text{(II. 24)}$$

Where μ and λ are the mean and shape parameters.

II.2.3.3 Compound Pareto distribution

Modelling the speckle component of the envelope detector using Rayleigh distribution gives the following expression:

$$p(x/y) = \frac{2x}{2\sigma^2+y} exp\left(-\frac{x^2}{2\sigma^2+y}\right) \quad \text{(II. 25)}$$

The Pareto-compound plus noise written as shown:

$$p(x) = \int_{\mathbf{0}}^{+\infty} \frac{2x}{2\sigma^2 + y} exp\left(-\frac{x^2}{2\sigma^2 + y}\right) \times \frac{b^v y^{-v-1}}{\Gamma(v)} exp\left(-\frac{b}{y}\right) dy \qquad (II.26)$$

II.2.3.4 Compound Log-Normal distribution

Obtaining the expression of CLN by considering the log normal as a texture, the CLN plus noise written as follow:

$$p(x) = \int_{0}^{+\infty} \frac{x}{\sigma^2 + 2y^2/\pi} exp\left(-\frac{x^2}{2\sigma^2 + 4y^2/\pi}\right) \times \frac{1}{\sqrt{2\pi}\ \sigma y} \exp\left(\frac{(\ln(y) - \mu)^2}{2\sigma^2}\right) \qquad (II.27)$$

II.2.3.5 CIER distribution

Recently, in [Chalabi2023] the CIER distribution is proposed, this distribution is based on the use of the inverted Exponentiated Rayleigh distribution as texture component. The IER PDF is given as [Gao2019]:

$$p(y) = 2\alpha\beta y^{-3}\ exp\left(-\frac{\beta}{y^2}\right)\left(1 - exp\left(-\frac{\beta}{y^2}\right)\right)^{\alpha-1}, y > 0 \qquad (II.28)$$

Where $\alpha > 0$ and $\beta > 0$ are the shape and the scale parameters.

Substituting the IER texture component (II.28) and the speckle (II.22) into (II.8), the CIER distribution PDF is obtained as:

$$p(x) = \int_{0}^{+\infty} \frac{2\alpha\beta x y^{-3}}{\sigma^2 + 2y^2/\pi}\ exp\left(-\frac{x^2}{2\sigma^2 + 4y^2/\pi} - \frac{\beta}{y^2}\right)\left(1 - exp\left(-\frac{\beta}{y^2}\right)\right)^{\alpha-1} dy \qquad (II.29)$$

The CCDF provides the probability that clutter returns will surpass a specified detection threshold T, obtained the CCDF from (II.29) as follow:

$$CCDF(T) = \int_{0}^{+\infty} 2\alpha\beta y^{-3}\ exp\left(-\frac{T^2}{2\sigma^2 + 4y^2/\pi} - \frac{\beta}{y^2}\right)\left(1 - exp\left(-\frac{\beta}{y^2}\right)\right)^{\alpha-1} dy \qquad (II.30)$$

For the special case $\alpha = 1$, the IER distribution (II.31) becomes inverse Rayleigh [Voda1972], the IR's distribution PDF is given as:

$$p(y) = 2\theta y^{-3} exp\left(-\frac{\theta}{y^2}\right)^{\alpha-1}, y > 0 \qquad (II.31)$$

Where $\theta > 0$ is the scale parameter.

Using the IR distribution as the texture component in equation (II.8) produces the compound inverted Rayleigh. The resulting PDF depends on two parameters and is expressed as:

$$p(x) = \int_0^{+\infty} \frac{2x\theta y^{-3}}{\sigma^2+2y^2/\pi}\, exp\left(-\frac{x^2}{2\sigma^2+4y^2/\pi} - \frac{\theta}{y^2}\right) dy \qquad (II.32)$$

The CCDF of CIR distribution is expressed from (II.32) as follow:

$$CCDF(T) = \int_0^{+\infty} 2\theta y^{-3}\, exp\left(-\frac{T^2}{2\sigma^2+4y^2/\pi} - \frac{\theta}{y^2}\right) dy \qquad (II.33)$$

II.3 Conclusion

In this chapter, the Modelling of the sea clutter is considered where the behavior of this kind of clutter is explained. This type of clutter has non Gaussian nature and its PDF is characterized by heavy tail. Several non-Gaussian distributions are presented in this chapter according to three categories; simple models like Weibull and log normal and gamma distributions. Also, the compound models in both cases presence and absence of thermal noise such as CK, CIG and CIER. The expressions of the PDFs and the CCDFs of these distributions are also reminded.

Chapter III: High-resolution sea clutter modelling analyses

III.1 Introduction

This chapter is focused to assess the modelling performance of CIER disribution in presence of thermal noise, the performances are compared with the well known compound K distribution and the CIG distribution using high-resolution sea clutter collected by McMaster University, Canada, IPIX radar [Bakker and Currie]. The ability to fit the real PDF and CCDF of the real data is checked for different data sets according to the different resolutions and polarizations, the real PDF curve is obtained using Kernel smoothing density estimation method given in [Bowman1997], this method is exsist in Matlab by using the 'ksdensity' function. The parameters of all distributions are estimated using the curve fitting estimation method based on the unconstraint Nelder-Mead algorithm [Mezache2011]. Modelling efficiency of the proposed model is evaluated using the mean square error and the Kolmogorov–Smirnov criteria.

III.2 IPIX radar database

IPIX is experimental and X-band radar works according to dual polarizations of its antenna. The IPIX radar is located in Grimsby, Ontario, Canada, at an elevation of 20 m above the level of Lake Ontario. It operates in the X frequency band with an antenna beam width of 9°. Its pulse repetition frequency is 1 kHz. This database is characterized by 34 resolution cells and 60,000 pulses. The data are available in three resolutions 3, 15 and 30 m. the different features of the IPIX radar are presented below [Bakker and Currie]:

a) Key Features

- X-band - 3cm wavelength
- Fully Coherent
    - Doppler measurements
    - clutter suppression
- Dual Linear Polarization
    - pulse-to-pulse transmit switching
    - simultaneous dual polarization on receive
    - full polarization matrix with two pulses
- Pulse Compression
    - 5 meter resolution
    - increased average power
- Arbitrary Transmit Waveforms
    - 25 MHz bandwidth

- Multi-Frequency Operation
    - dual simultaneous transmit frequencies
    - frequency agility
    - resolve scales down to 30 cm
    - above features result in an increased range resolution and an increased number of independent samples for better reflectivity and Doppler spectrum estimates
- Computer control
    - extremely flexible configuration
- Digital Data Acquisition
    - raw data archived
- External/Internal Calibration
- In-Field Real-Time Analysis and Display Capability
- Transportable
    - 40 foot equipment trailer
    - separate antenna pedestal/trailer

b) Transmitter Specifications

Type	Travelling Wave Tube Amplifier
Frequency	9.39 GHz (fixed)
	8.9 to 9.4 GHz (agile)
Peak power	8 KW
Pulse Length	20 ns to 5000 ns (real)
	5000 ns (expanded)
	32 ns (compressed)
PRF	0 to 20 KHz
Polarization	Linear, H or V
	Pulse-to-pulse switchable

c) Receiver Specifications

Number	2
Outputs	Linear, I and Q
Signal	H or V
	Fixed or agile
BW	5.5 MHz (Gaussian)
	50 MHz (chirp)
	100 MHz
Noise figure	1.2 dB

Minimum range	150 m typ.
Sensitivity	10 dBZ at 150 Km
	-35 dBZ at 10 km vert cloud profile

d) Antenna Specifications

Type	Linear dual-polarized
	Parabolic reflector
	Center fed
Size	2.4 m
Beamwidth	1.1 degrees
Gain	45.7 dB
Isolation	30 dB (X-pol)
Rotation	Elev. over azm.
	0 to 10 RPM (azm.)

e) Data Acquisition System

Sample rate	0 to 50 MHz
Outputs	Linear, I and Q
Quantization	8 or 10 bits - up to 16 bit effective with H/W decimation
Sample gating	Range, azimuth, elevation
Capacity	64 M samples

III.3 Curve fitting estimation method

The Nelder-Mead algorithm-based curve fitting method [Mezache2011] will be used to estimate the parameters of the different models. The Nelder-Mead simplex mathematical optimization algorithm was applied to optimize the MSE between the real curve and the estimated CDF curve. The estimated parameters are used to plot the estimated PDF and CDF curves in order to finally compare them with the plot of the real PDF and CDF, the PDF is obtained by the Kernel Smoothing estimate method [Bowman1997]. This procedure for simultaneously estimating the three parameters is applied in real time and executed according to the flowchart below (Fig III.1).

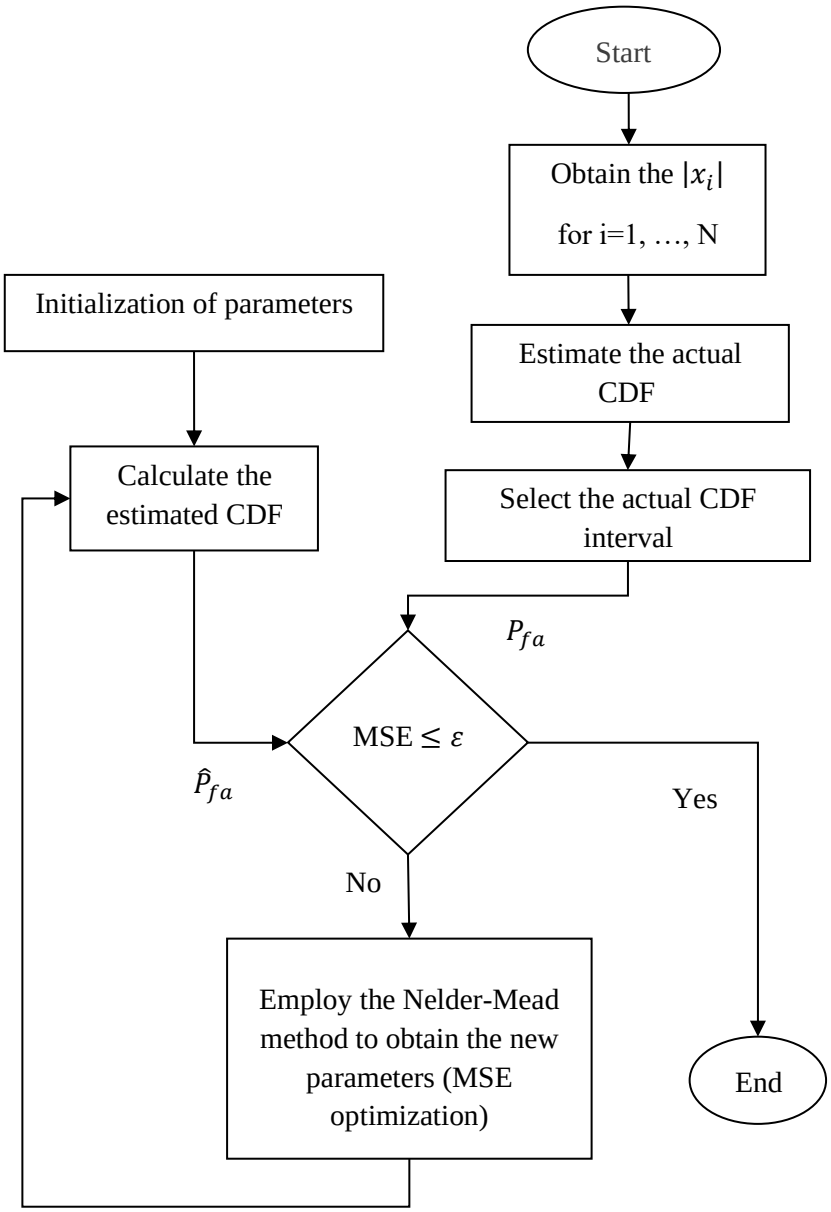

Figure III.1: Flowchart of curve fitting method

III.4 Results and discussion

In this sub-session, the modelling performance is assessed using the real data described in the previous session. First, table III.1 contain the estimated parameters of the CK, CIG, CIR and CIER distributions obtained using the curve fitting method. These parameters will be used to plot the PDFs and CDFs curves.

The Figure III.2 show the CIER amplitude PDF for b = 1, σ = 0.5 and different values of shape parameter α = 0.1, 1, 10. It is clear that the CIER is non Gaussian and a heavy-tailed distribution, the increase of the shape parameter yeld that the CIER distribution tends to a Rayleigh distribution.

For HH polarization, 10th range of cells and resolution 3 m, the real and the estimated PDFs and CCDFs are plotted in Figure III.3, from this figure it is clear that the CIER and the CIR PDFs and CCDFs provide a good fit to the real PDF and CCDF compared to the compound K and CIG distributions, this is very clear in the tail region. From Table III.2, the CIR have the lowest value of the PDF MSE and KS test but for the CCDF the CIG offers the lowest values. The PDFs and the CCDFs curves illustrated in Figure III.4 are obtained from the HH polarization, 8th range of cells and resolution 15 m, The CIER distribution leads the best fit to the real data with the best MSE and KS values.

In the other hand, for VV polarization, the 32th range of cells and resolution 3 m in Figure III.5 shows that the CIER model gives the best fit according to the minimum values of MSE and KS followed by the CIR distribution. For the same polarization, the Figure III.6 is obtained by using the 34th range of cells and with 15 m resolution, the results confirm the ability of the CIER distribution to model high-resolution sea clutter. The curves represented in Figure III.7 are plotted using the data set of VV polarization, 20th range of cells and resolution 30 m, in this experiment, the best fit is achieved by the CIG and CEIR models. On the other hand, it is remarkable that the PDF and CCDF of the CIR deviate from the real PDF and CCDF at the tail region. The several performed tests confirm the modelling efficiency of the CIER model and their ability to model high-resolution sea clutter.

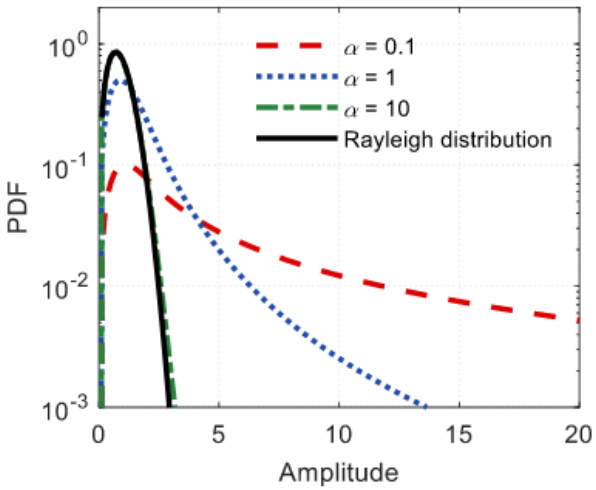

Figure III.2: Plots of the amplitude of PDF for CIER distributed clutter with β =1 and σ = 0,5.

Distribution	**parameters**	HH, 3m; 10th	HH, 15m, 8th	VV, 3m, 32th	VV, 15m, 34th	VV, 30m, 20th
CK	v	0.6960	0.4883	0.6583	0.5082	0.8027
	b	1.4917	0.9907	1.4495	1.0264	1.2134
	$2\sigma^2$	0.5031	-0.3494	0.5410	-0.2966	-0.3688
CIG	λ	0.5626	0.7922	0.8289	0.7640	3.3570
	μ	0.4001	0.5711	0.4331	0.5728	0.7332
	$2\sigma^2$	0.5455	0.3699	0.5667	0.3141	-0.2731
CIR	θ	0.0502	0.1313	0.0476	0.1384	0.1293
	$2\sigma^2$	0.5613	0.3603	0.5976	-0.2899	0.4300
CIER	α	1.3341	1.3362	1.5856	1.2600	2.7724
	β	0.3426	0.5032	0.4084	0.4794	0.9188
	$2\sigma^2$	0.5291	0.2957	0.5516	0.2318	-0.0303

Table III.1: Parameter Estimates of the Different distributions.

Data		Distributions			
		CK	CIG	CIR	CIER
Polarization: HH, 10th range of cells and resolution 3 m	MSE of PDFs	$1.4033X\ 10^{-4}$	$4.8035X\ 10^{-5}$	$3.9437X\ 10^{-5}$	$4.0203X\ 10^{-5}$
	KS value of PDFs	0.2700	0.1250	0.0750	0.0500
	MSE of CCDFs	$1.6980X\ 10^{-5}$	$2.2844X\ 10^{-6}$	$3.1278X\ 10^{-6}$	$2.3560X\ 10^{-6}$
	KS value of CCDFs	0.2226	0.2226	0.2392	0.2226
Polarization: HH, 8th range of cells and resolution 15 m	MSE of PDFs	0.0010	$8.7470\ X\ 10^{-5}$	$1.0263X\ 10^{-4}$	$6.8987X\ 10^{-5}$
	KS value of PDFs	0.1700	0.0500	0.1550	0.0650
	MSE of CCDFs	$1.8286X\ 10^{-4}$	$3.5058X\ 10^{-6}$	$8.9799X\ 10^{-6}$	$2.4475X\ 10^{-6}$
	KS value of CCDFs	0.2957	0.2957	0.2957	0.2957
Polarization: VV, 32th range of cells and resolution 3 m	MSE of PDFs	$8.8341X\ 10^{-4}$	$7.8161X\ 10^{-4}$	$7.7656X\ 10^{-4}$	$7.5224X\ 10^{-6}$
	KS value of PDFs	0.1050	0.1100	0.2300	0.1250
	MSE of CCDFs	$1.1810X\ 10^{-4}$	$6.9573X\ 10^{-5}$	$5.9513X\ 10^{-5}$	$5.1855X\ 10^{-5}$
	KS value of CCDFs	0.4186	0.4186	0.4186	0.4186
Polarization: VV, 34th range of cells and resolution 15 m	MSE of PDFs	0.0012	$2.0958X\ 10^{-4}$	$1.9891X\ 10^{-4}$	$1.0578X\ 10^{-4}$
	KS value of PDFs	0.2550	0.1050	0.0500	0.0850
	MSE of CCDFs	$1.7768X\ 10^{-4}$	$1.4124X\ 10^{-5}$	$1.3631X\ 10^{-5}$	$1.7286X\ 10^{-6}$
	KS value of CCDFs	0.2658	0.2658	0.2658	0.2658
Polarization: VV, 20th range of cells and resolution 30 m	MSE of PDFs	$7.1741X\ 10^{-5}$	$5.5953X\ 10^{-5}$	$4.2132X\ 10^{-4}$	$5.4942X\ 10^{-5}$
	KS value of PDFs	0.1100	0.0600	0.2500	0.0600
	MSE of CCDFs	$1.9355X\ 10^{-6}$	$5.6687X\ 10^{-7}$	$3.8928X\ 10^{-5}$	$5.6940X\ 10^{-7}$
	KS value of CCDFs	0.3688	0.3688	0.3688	0.3688

Table III.2: MSE and KS of PDFs and CCDFs for different data and types of distribution.

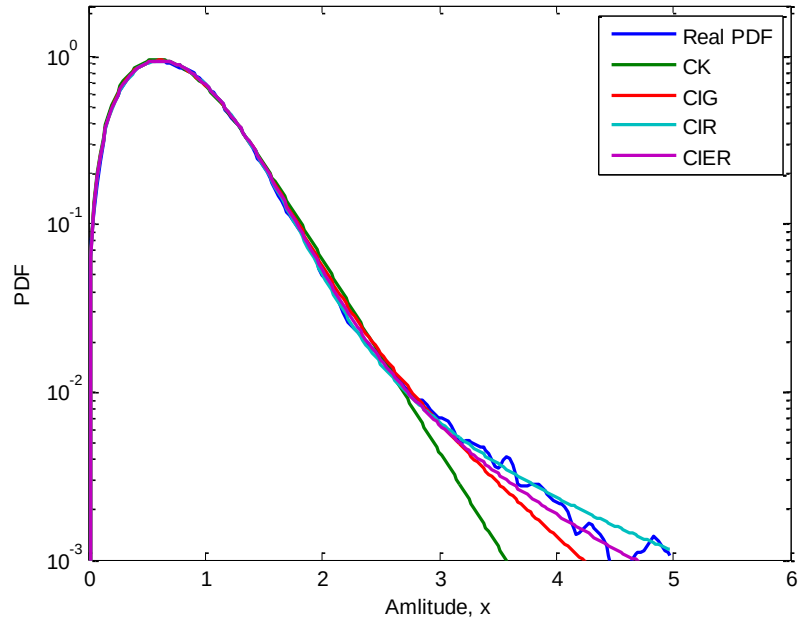

(a)

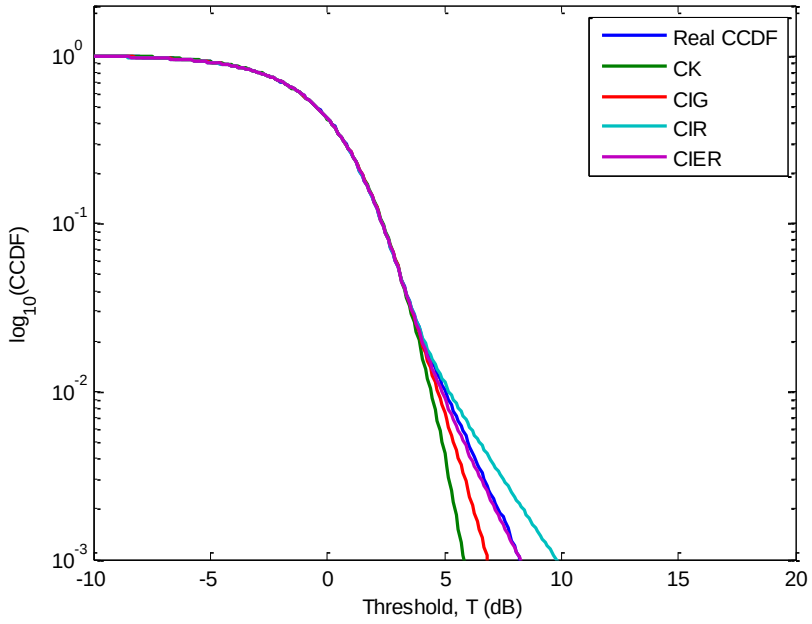

(b)

Figure III.3: Fitted (a) PDFs and (b) CCDFs for HH polarization, 10th range of cells and resolution 3 m.

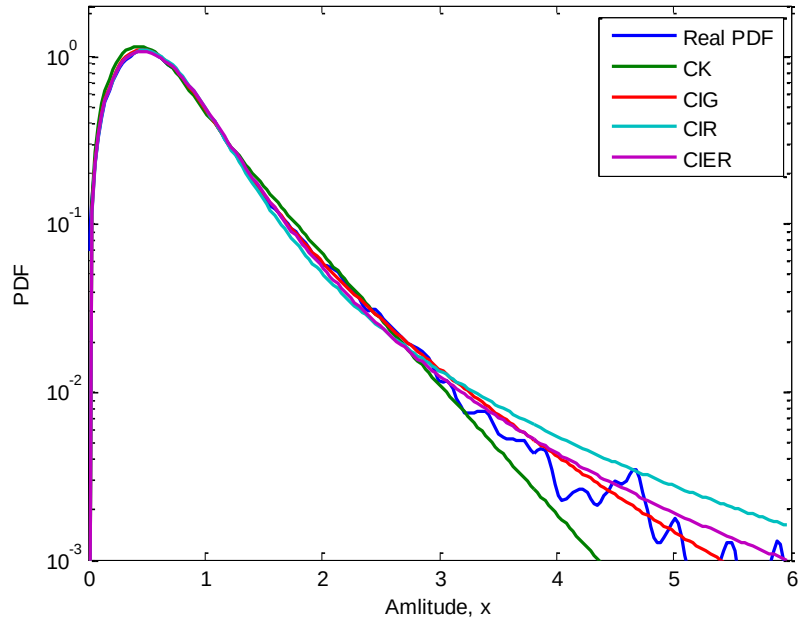

(a)

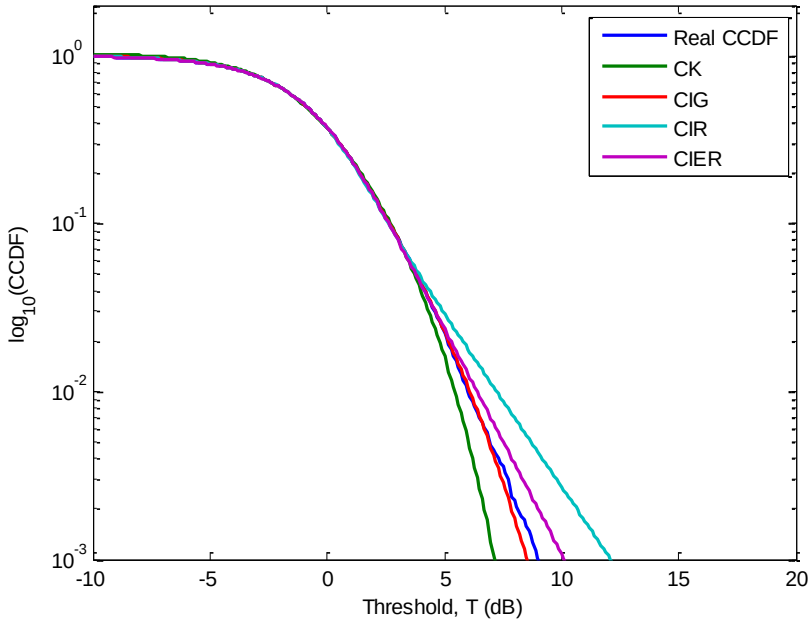

(b)

Figure III.4: Fitted (a) PDFs and (b) CCDFs for HH polarization, 8th range of cells and resolution 15 m.

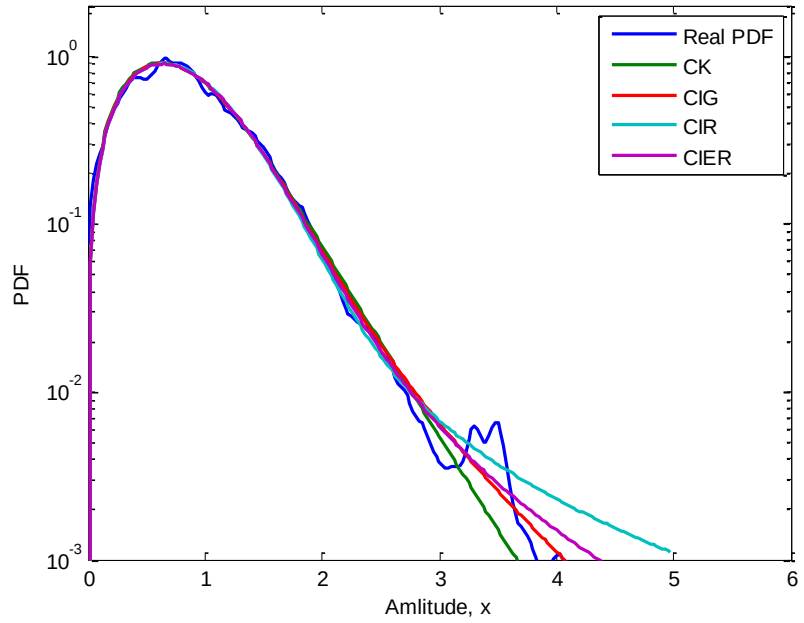

(a)

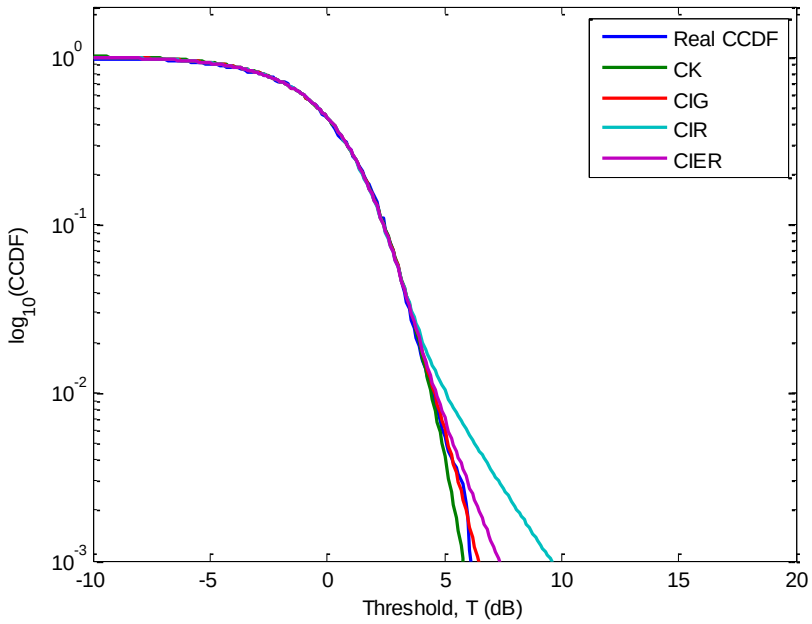

(b)

Figure III.5: Fitted (a) PDFs and (b) CCDFs for VV polarization, 32th range of cells and resolution 3 m.

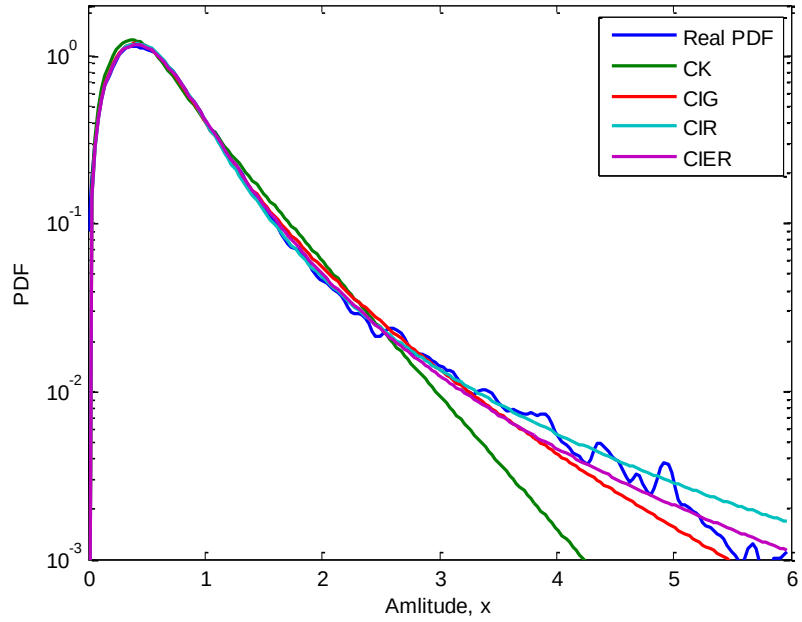

(a)

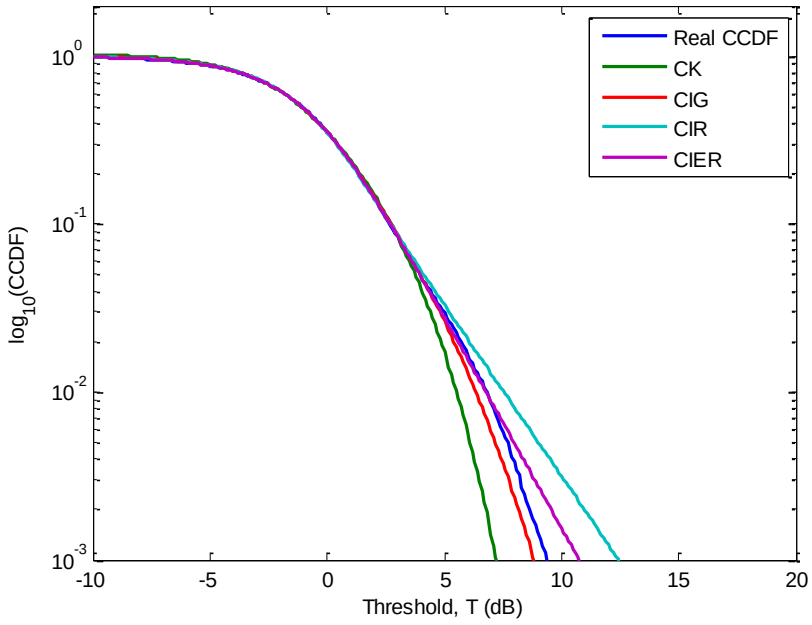

(b)

Figure III.6: Fitted (a) PDFs and (b) CCDFs for VV polarization, 34th range of cells and resolution 15 m.

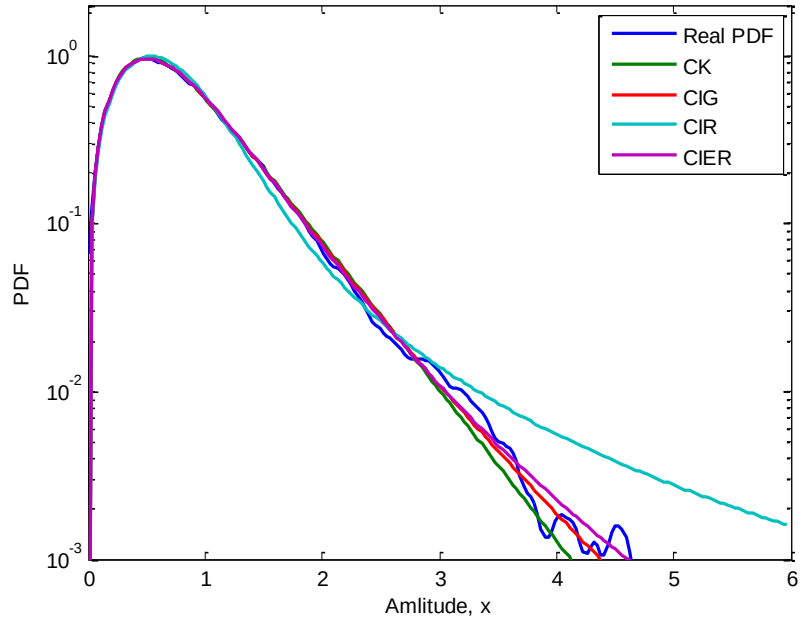

(a)

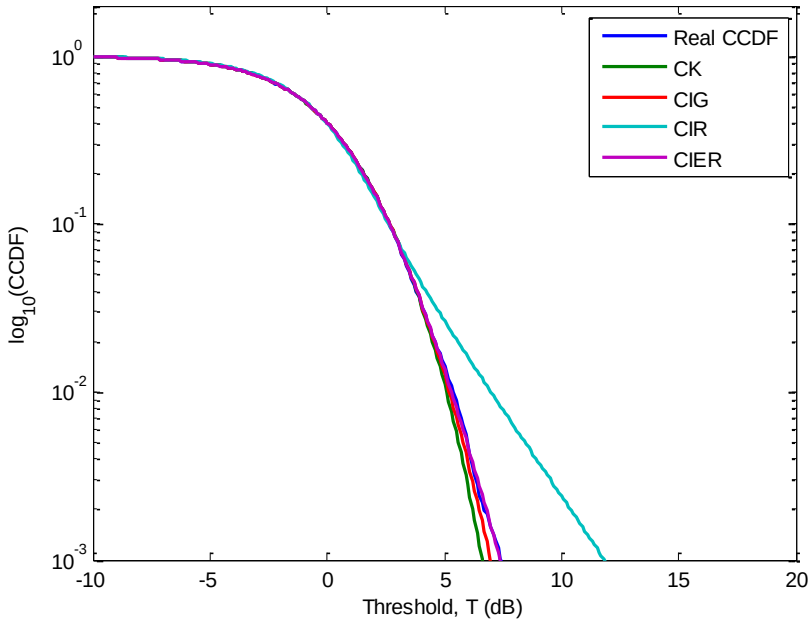

(b)

Figure III.7: Fitted (a) PDFs and (b) CCDFs for VV polarization, 20th range of cells and resolution 30 m.

III.5 Conclusion

In this chapter, a comparative study of high-resolution sea clutter modelling in presence of thermal noise is established. The modelling performance is evaluated by plotting the PDFs and the CCDFs curves of the considered distributions CK, CIG, CIER, CIR and the empirical PDF and CCDF of the data. The real data used in this study are collected by the IPIX radar in maritime environment. Several tests are performed according different data range cells and different polarizations and resolutions. The results indicate the ability of the CIER model to model this kind of clutter, this is illustrated by the lowest MSE and KS values compared to the compound K, CIG and the CIR distributions.

General conclusion

General conclusion

High resolution sea clutter modelling is pivotal issue in the development of performant CFAR detectors. Worse modelling of the clutter yield to an important increase of false alarm rate and degradation of the detection performance. Several work have been proved that the sea clutter have non Gaussian nature. In chapter II, the radar signal interaction mechanisms is explained and the different distributions used to model the sea clutter are reminded and categorized in three types; simple models such as Log-normal and the Weibull distributions. The compound models in both cases of presence and absence of thermal noise like the k distribution, CIG and CIER. In chapter III, the modelling performance of the CIER distribution including the thermal noise is assessed. Several tests have been performed using the IPIX database where the fitted PDFs and the CCDFs of the CIER, compound K, CIG and the special case CIR distributions are compared with the real PDF and CCDF. The results obtained validate the ability of the CIER distribution to model high-resolution sea clutter.

Bibliography

1. [Baker1985] BAKER, C. J. et WARD, K. D.,“ Coherent and noncoherent properties of Kdistributed sea clutter,” RSRE Research Review, 1985, p. 31-33.

2. [Bakker and Currie] Bakker, R. B., and B. Currie. The McMaster IPIX Radar Sea Clutter Database, Online available: http://soma.crl.mcmaster.ca/ipix

3. [Barkat2005] Barkat, M., “Signal Detection and Estimation, 2nd ed.” Artech House, Boston, London, 2005.

4. [Bowman1997] Bowman, A. W., and A. Azzalini. 1997. Applied Smoothing Techniques for Data Analysis. New York:Oxford University Press.

5. [Chalabi2015] Chalabi, I., and Mezache, A., “Sea clutter modeling in presence of thermal noise using beta-prime texture distribution,” IEEE Conference Publications. Systems, Signals & Devices (SSD), 2015 12th International Multi-Conference, Tunisia, 2015.
6. [Chalabi2016] Izzeddine Chalabi "Estimation et Détection Adaptative des Cibles pour Radars MIMO dans un Environnement de Clutter non-Gaussien " Doctorat these UNIVERSITE DE MOHAMED BOUDIAF-M’SILA FACULTE DE TECHNOLOGIE DEPARTEMENT D’ELECTRONIQUE.ch2, 2016-2016, pp 15.

7. [Chalabi2023] Izzeddine Chalabi (2023) High-resolution sea clutter modelling using compound inverted exponentiated Rayleigh distribution, Remote Sensing Letters, 14:5, 433-441, DOI: 10.1080/2150704X.2023.2215894

8. [Echard1991] Echard, J., “Estimation of Radar Detection and False Alarm Probabilities,” IEEE Transactions on Aerospace and Electronic Systems, Vol. 27, PP. 255-260, March 1991.

9. [Farina1997] Farina, A., Gini, F., Greco, M.V., and Verrazzani, L., “High resolution sea clutter data : statistical analysis of recorded live data,’’ IEE Pro-Radar. Sonar Navig. Vol. 144, N°. 3, June 1997.

10. [Fay1977] Fay, F. A., Clarke, J., and Peters, R. S., “Weibull distribution applied to sea clutter,” IEE International Conference Radar ’77, (London, UK), pp. 101-104, October 1977.

11. [Farshchian2010] Farshchian, M., and Posner, F. L., “The Pareto distribution for low grazing angle and high resolution X-band sea clutter,” Proceedings of IEEE Radar Conference., Arlington, VA, USA, pp. 789-793, 2010

12. [Gao2019] Gao, S., and W. Gui. 2019. “Parameter Estimation of the Inverted Exponentiated Rayleigh Distribution Based on Progressively First-Failure Censored Samples.” International Journal of System Assurance Engineering & Management 10 (5): 925–936. Doi:10.1007/s13198-019-00822-9.

13. [Gandhi1994] Gandhi, P. P., and Kassam, S. A., “Optimality of the cell averaging CFAR detector,” IEEE Transactions on Information Theory, Vol. 40, N°4, pp. 1226-1228, July 1994.

14. [Goldstein1973] Goldstein, G.B., “False-alarm regulation in log-normal and Weibull clutter,” IEEE Transactions on Aerospace and Electronic Systems, Vol. 9, N°. 1, pp. 84-92, January 1973.

15. [Gini2000] Gini, Fulvio, et al. "Performance analysis of two adaptive radar detectors against non-Gaussian real sea clutter data." *IEEE Transactions on Aerospace and Electronic Systems* 36.4 (2000): 1429-1439.

16. [Greco2004] Greco, Maria, Federica Bordoni, and Fulvio Gini. "X-band sea-clutter nonstationarity: Influence of long waves." *IEEE Journal of Oceanic Engineering* 29.2 (2004): 269-283.

17. [Guida1993] Guida, M., Longo, M., and Lops, M., “Biparametric CFAR procedures for Lognormal clutter,”IEEE Transactions on Aerospace and Electronic Systems, Vol. 29, N°3, pp. 798-809, July 1993.

18. [Haykin2002] Haykin, S., Bakker, R., and Currie, B. W., ‘’Uncovering nonlinear dynamics the case study of sea clutter data,” Porc. IEEE, Vol. 90, pp 860881, May 2002.

19. [Jakeman1976] Jakeman, E., and Pusey, P. N., “A model of non-Rayleigh sea echo,” IEEE Transactions on Antennas and Propagation, Vol. 24, N°. 6, pp. 806-914, November 1976.

20. [Lewinski1983] Lewinski, D. J., “Nonstationary probabilistic target and clutter scattering models,” IEEE Transactions on Antennas Propagation, Vol. 31, N°. 3, 480-498, 1983.

21. [Mahafza2003]. Bassem R. Mahafza, Atef Z. Elsherbeni "MATLAB simulations for radar systems design"Library of Congress Cataloging-in-Publication Data, vol.01.2003, pp.13-14-15.

22. [Mezache2011] Mezache, A., Sahed, M., Laroussi, T., and Chicouche, D., “Two novel methods for estimating the compound K-clutter parameters in presence of thermal noise,” IET Radar, Sonar and Navigation, Vol. 5, N°9, pp. 934-942, 2011.

23. [Mezache2015] Mezache, A., Sahed, M., Soltani, F., and Chalabi, I., "Model for non-Rayleigh Clutter Amplitudes Using Compound Inverse Gaussian Distribution: An Experimental Analysis" IEEE Transactions on Aerospace and Electronic Systems, Vol. 51, N°. 1, pp. 142-153, January 2015.Doi:10.1109/TAES.2014.130332.

24. [Richards2010] Richards, M. A., Scheer, J. A., & Holm, W. A. (2010). Principles of Modern Radar: Basic Principles (Vol. I). SciTech Publishing.

25. [Richards2014] Richards, M. A., Scheer, J. A., & Holm, W. A. (2014). Principles of Modern Radar: Basic Principles. SciTech Publishing.

26. [Rosenberg2013] Rosenberg, L., and Bocquet, S., "The Pareto distribution for high grazing angle sea clutter," IEEE International Geoscience and Remote Sensing Conference, Melbourne, Australia, pp. 4209-4212, 2013.

27. [Schleher1976] Schleher, D. C., "Radar detection in Weibull clutter," IEEE Transactions on Aerospace and Electronic Systems, Vol. 12, N°. 6, pp. 736-743, November 1976

28. [Sekine1990] Sekine, Matsuo, and Yuhai Mao. Weibull radar clutter. No. 3. IET, 1990.

29. [Trunk1978] Trunk, G. V., "Range resolution of targets using automatic detection," IEEE Transactions on Aerospace and Electronic Systems, Vol. 14, N°. 5, pp. 750-755, September 1978.

30. [Verheij2000] Verheij, L. F., & Holthuijsen, L. H. (2000). A wave prediction model for the computation of the radar cross-section of the ocean surface. *IEEE Transactions on Geoscience and Remote Sensing*, 38(1), 88-98.

31. [Voda1972] Voda, V. G. 1972. "On the Inverse Rayleigh Distributed Random Variable." Reports of Statistical Application Research 19 (4): 13–21.

32. [Ward1981] Ward, K. D., "Compound representation of high resolution sea clutter," Electronics Letters, Vol.17, N°. 16, pp. 561-563, August 1981.

33. [Ward1982] Ward, K. D., "A radar sea clutter model and its application to performance assessment," IEE Conference Publication, pp. 203-207, October 1982.

34. [Watts1985]Watts, S., "Radar detection prediction in sea clutter using the compound K distribution model," IEE Proceedings, Part F, Vol. 132, N°. 7, pp. 613-620, December 1985.

35. [Watts1987] Watts, S., "Radar detection prediction in K-distributed sea clutter and thermal noise," IEEE Transactions on Aerospace and Electronic Systems, Vol. 23, N°. 1, pp. 40-45, January 1987. doi:10.1109/TAES.1987.313334.

36. [Weinberg2013] Weinberg, G.V., "Estimation of Pareto clutter parameters using order statistics and linear regression," Electronics Letters, Vol. 49, N°. 13, pp. 845-846, June 2013.

37. [Weiss1982] Weiss, M., "Analysis of Some Modified Cell-Averaging CFAR Processors in Multiple Target Situations," IEEE Transactions on Aerospace and Electronic Systems, Vol. 18, N°. 1, pp. 102-114, January 1982.